Effect of Porosity on Transverse Weld Fatigue Behavior

Fatigue lives of GMA butt welds in 5083 aluminum are related to the cross sectional area of the pores responsible for fatigue crack initiation

BY R. C. ANDREW AND J. WARING

ABSTRACT. This paper outlines a method for determining the cross-sectional area of the pore(s) or group(s) of pores which nucleated cracking in transverse weld test-pieces under flexural bending fatigue conditions. Flexural bending fatigue life at constant amplitude is shown to be directly related to the cross sectional area of the crack nucleating pores, the average crack nucleating site area increasing with increasing welding speed.

Introduction

Even though it is widely recognized that porosity is present to some extent in all aluminum alloy welds, few attempts have been made to relate weld fatigue behavior to weld porosity content. Several investigators have qualitatively stated that porosity is responsible for a serious reduction of weld fatigue properties (Refs. 1,2). Rupert and Rudy (Refs. 3,4) reported that the axial tension fatigue lives at constant stress levels of gas tungsten-arc (GTA) welds in the aluminum alloys 2219-T87 and 2014-T6 decreased at a logarithmic rate as the porosity content, measured in terms of the area of porosity present on a fracture surface, increased. An investigation by Shore (Ref. 5) into the effect of porosity on the fatigue strength of ½ in. thick plates of 7039-T6151 gas metal-arc (GMA) welded with 5039 filler metal and then naturally aged for a minimum of 30 days produced results similar to those of Rupert and Rudy.

Although these two investigations disclosed useful quantitative information about the influence of area of porosity on fatigue strength, both works suffer certain limitations. Porosity was deliberately introduced into the welds by artificially contaminating the shielding gas with either water vapor or hydrogen in order to produce measurable quantities of porosity. Notwithstanding that this allows the operator a degree of control over weld gas content, the results obtained cannot be directly related to actual weld performances because of the artificial porosity, to some extent, masks any dependence of fatigue strength on the porosity normally present in commercially welded joints.

Secondly, only a limited pore size range has been considered with emphasis placed upon pores greater than 1/64 in. diam. Little was done quantitatively to evaluate the effects on fatigue behavior of the large amounts of fine porosity (less than 1/64 in. diam) frequently present in the welds. Thirdly, the influence of porosity on fatigue strength was determined wholly in terms of the total pore area visible on the fracture surface with little emphasis being placed upon pore location and distribution effects. Finally, the fatigue testing was restricted to axial loading.

Experimental Details

A survey of the literature disclosed that welding conditions markedly affect the porosity content of aluminum alloy welds (Refs. 6,7). Consequently, in order to obtain a range of weld porosity levels three series of welds were made, the major variable in each series being the arc travel speed. The 5083 base metal plates (0 temper) were in the form of rolled stock cut to welding samples of 24 × 6 × 3/16 in. (4.8 mm) thick. All welds were full penetration, single pass, butt welds laid in the flat position parallel to the rolling direction, i.e., along

R. C. ANDREW is Research Officer and J. WARING is a Senior Lecturer, Dept. of Mining and Metallurgical Engineering, University of Queensland, Australia.

the 24 in. length. The filler metal was 1/16 in. (1.6 mm) diam 5356. The GMAW torch was rigidly fixed at 15 deg forehand angle above the moving workpieces, arc travel speed being controlled by a hydraulically actuated table (Fig. 1).

The first two series of welds (designated Series A and Series B) were made at intervals of 5 ipm in the welding speed range 10-50 ipm (0.42-2.11 cm/sec). The base metal plates used for the Series A and Series B welds were degreased with acetone and then, immediately prior to welding, the edges to be abutted and the adjacent top and bottom surfaces were stainless steel wire brushed. Care was taken that all cleaned surfaces were maintained scrupulously free of contaminants (fingerprints, grease, oil, etc.).

The third series of welds (Series C) was also made at intervals of 5 ipm in the welding speed range of 10-50 ipm (0.42-2.11 cm/sec). However, a different method of base metal edge preparation was used for these Series C welds in an attempt to reduce the porosity content below that of the Series A and B welds (Refs. 8,9). Immediately before welding, each plate was degreased with acetone, stainless steel wire brushed, and the edges to be abutted were then milled in the absence of any lubricant. The actual Series C welding conditions were similar to those for the Series A and B welds. Commercial welding grade argon was used in all three weld series for gas shielding (99.95% purity, dew point −40 C). Further details of the welding procedures used are contained in Ref. 10.

Fatigue Testpiece Preparation

Six flexural bending fatigue testpiece blanks were obtained from each of the 27 welds. The reinforcement and underbead were removed from each testpiece blank by milling before the blanks were sawn to final shape. The edges of each testpiece were then machined smooth with a tungsten tipped router. A high speed power planer was used to remove any surface irregularities remaining after the milling operation and to produce smooth parallel faces on the fatigue testpieces. Adequate lubrication was provided and only small cuts (0.002 in.) were made during the milling, routing and planing operations so that the test piece surfaces would not work harden. After machining, the testpieces were hand polished with 400 grade wet and dry paper, care being taken to maintain the final series of scratches parallel to the longitudinal axes of the testpieces. The size and shape of the flexural bending fatigue testpieces are shown in Fig. 2.

The conditions operative for the flexural bending testing were:

1. Frequency: 500 cycles/min
2. Maximum amplitude: 0.625 in. (see Fig. 2.)
3. Criterion of failure: complete failure
4. Temperature: 20 C ± 2 C

A plan view of the flexural bending equipment is shown in Fig. 3.

Fracture Surface Examination

The flexural bending fatigue tests revealed an overall trend for the fatigue life at constant amplitude to decrease with increasing welding speed (Ref. 11). A number of these fatigue surfaces were selected at random for examination with an optical stereoscopic microscope in order to determine the location of the pore(s) or group(s) of pores responsible for the fatigue crack initiation (Ref. 10). A "Cambridge Stereoscan Mark II" electron microscope was then used to photograph the fatigue crack initiation sites located with the optical stereo-microscope. Parallax error was overcome and a plan view of the fatigue crack initiating site(s) was obtained by positioning the fracture surface in the specimen chamber of the scanning electron microscope so that the incident electron beam was normal to the fracture surface, i.e. "zero tilt."

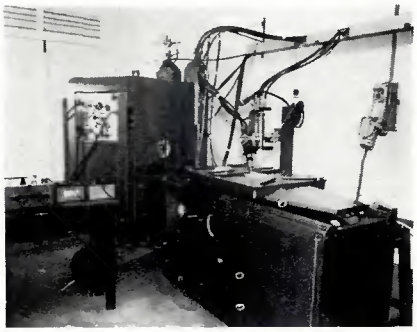

Fig. 1 — The relative positions of the hydraulically actuated welding table and the power source

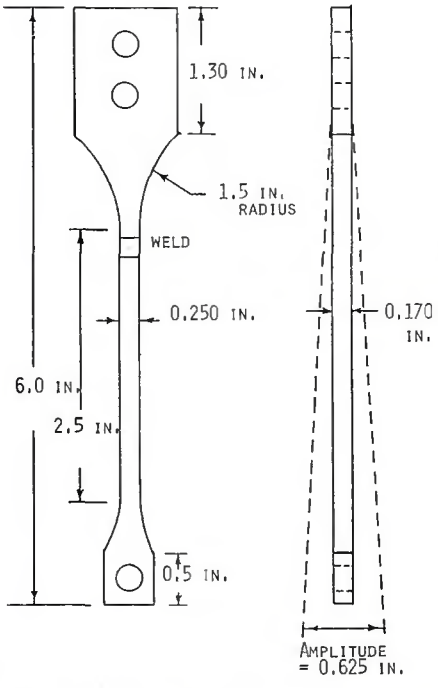

Fig. 2 — Shape and dimensions of the flexural bending fatigue testpiece, showing also the deflection amplitude employed

The area of each initiation site photographed was traced out with a planimeter. The pores responsible for fatigue crack initiation occurred in a wide variety of combinations. When single pores were responsible for fatigue crack initiation, their cross sectional area was easily determined by measuring the area enclosed within the pore circumference. If a group of pores was responsible for fatigue crack initiation, a boundary line enclosing all the pores in the group was drawn and the area contained within this boundary line used as a measure of the crack initiation site cross sectional area. When more than one crack initiation site was present on a fracture surface, the cross sectional area of each individual site was assessed and then summed to provide a total initiation site cross sectional area value for this fracture surface.

In order to verify that the pores responsible for fatigue crack nucleation were approximately bisected by the spread of the fatigue crack, the mating fracture surfaces from a number of flexural bending testpieces were compared. In all cases the pore(s) exposed on one fracture surface, including those responsible for crack initiation, were almost a mirror image of those present on the mating surface. Consequently, quantitative crack initiation pore cross sectional area measurements were made on only one fracture surface from each testpiece.

Results

The slower welding speed testpiece failures generally started at a single initiation site, this being composed of a single pore or a group of two or three pores (Figs. 4 and 5). In marked contrast, the higher welding speed testpiece failures were each frequently initiated at up to six individual sites, each site containing a number of pores of varying sizes (Figs. 6 through 12). The pores responsible for the flexural bending fatigue failures were all located either at a surface of maximum stress, i.e. at the underbead or reinforcement surface, or within one pore diameter of such surfaces.

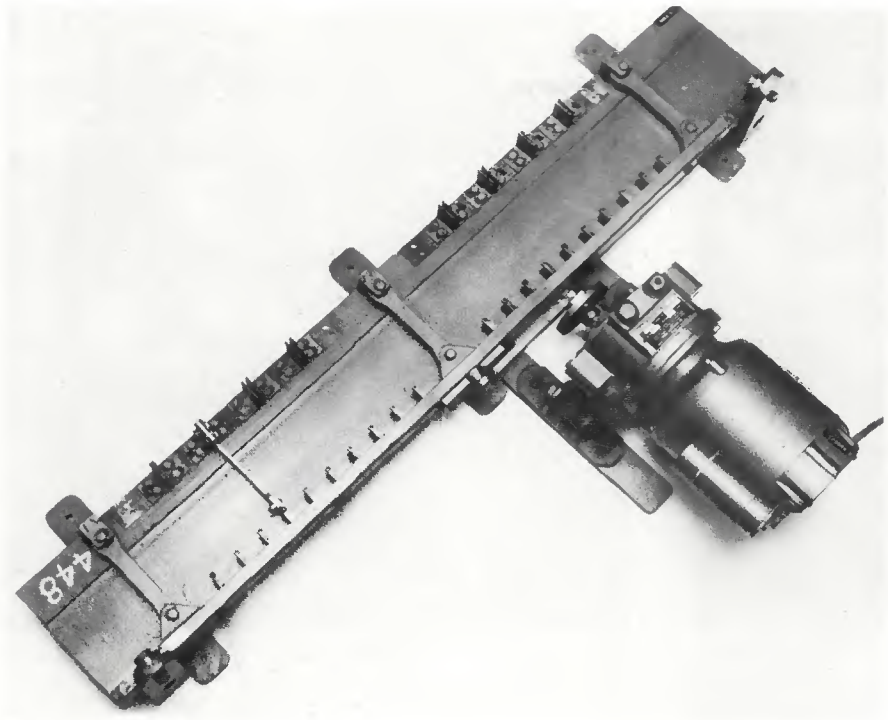

Fig. 3 — The flexural bending fatigue equipment showing one testpiece in place

Fig. 4 — The two pores (arrow) responsible for fatigue crack initiation in a slow speed Series C weld. Note the virtual absence of pores on the fracture surface. Welding speed = 15 ipm (0.64 cm/sec); angle of tilt = zero. (X21, reduced 13%)

Table 1 — Flexural Bending Fatigue Crack Initiation Site Cross Sectional Area Evaluation

Weld series	Welding speed, cm/sec	Initiating sites, no. & type	Cross sectional area, each site, $mm^2 \times 10^{-4}$	Total cross sectional area, $mm^2 \times 10^{-4}$	Cycles to failure
B	0.42	1 single pore	45.0	45.0	59,000
C	0.42	1 single pore	52.0	52.0	56,500
B	0.64	1 single pore	32.0	32.0	76,000
C	0.64	2 sites, each a single pore	45.0 45.0	90.0	37,000
B	0.85	3 sites, each a single pore	32.0 13.0 19.0	64.0	43,500
C	0.85	3 sites, each a single pore	39.0 39.0 6.0	84.0	44,500
C	1.06	1 site, several pores	1006.0	1006.0	16,000
C	1.27	2 sites, 1 of 1 pore, 1 of 6 pores	26.0 252.0	278.0	30,000
C	1.27	2 sites, 1 of 1 pore, 1 of many pores	13.0 239.0	252.0	32,000
C	1.48	1 site, many pores	226.0	226.0	33,000
B	1.48	3 sites, 1 of 1, 1 of 3 and 1 of 4 pores	45.0 51.0 400.0	496.0	21,000
C	1.69	1 group of 3 pores	277.0	277.0	30,000
B	2.11	6 sites, 1 of 1 pore, 1 of 2 pores, 1 of 3 pores, and 3 of many pores	97.0 187.0 39.0 348.0 58.0 103.0	832.0	19,500
C	2.11	5 sites, 2 of 1 pore each 1 of 3 pores, 1 of 4 pores, 1 of 6 pores	45.0 52.0 304.0 168.0 470.0	1039.0	13,500

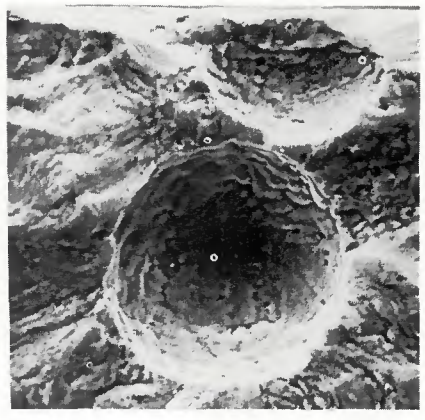

Fig. 5 — Higher magnification view of the two pores shown in Fig. 4. (X525, reduced 41%)

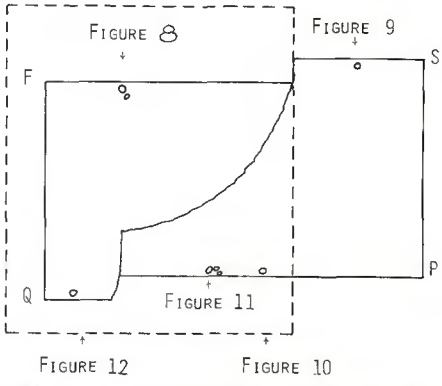

Fig. 6 — Diagrammatic representation of the fracture surface in Fig. 7 (broken line shows actual boundary). Magnified views of the pores are shown in the subsequent figures indicated

The overall number of pores on the faster welding speed fracture surfaces was considerably higher than that on the slower welding speed fracture surfaces — the pores on the higher welding fracture surfaces mainly occurring in groups while those on the slower speed surfaces occurred singly (compare Figs. 4 and 7). The total initiation site cross sec-

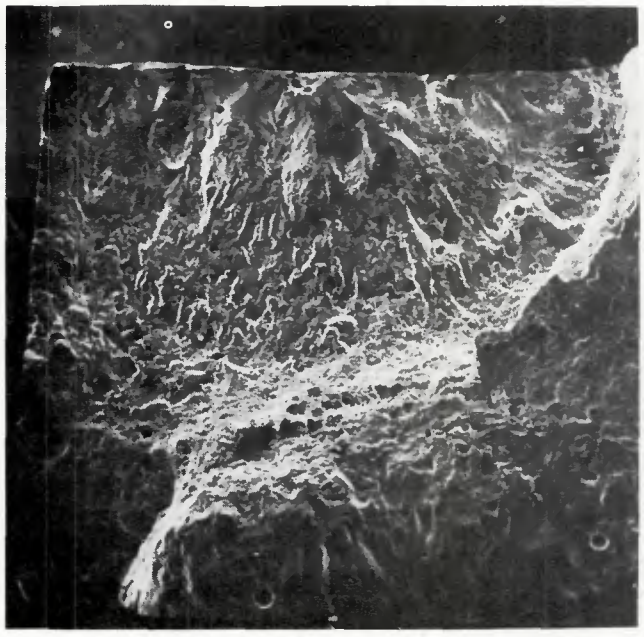

Fig. 7 — Plan view of a portion of the fracture surface of a fatigue testpiece from the fastest Series C weld. Note the large number of pores visible on the fracture surface. Welding speed = 50 ipm (2.11 cm/sec); angle of tilt = zero. (X 22, reduced 9%)

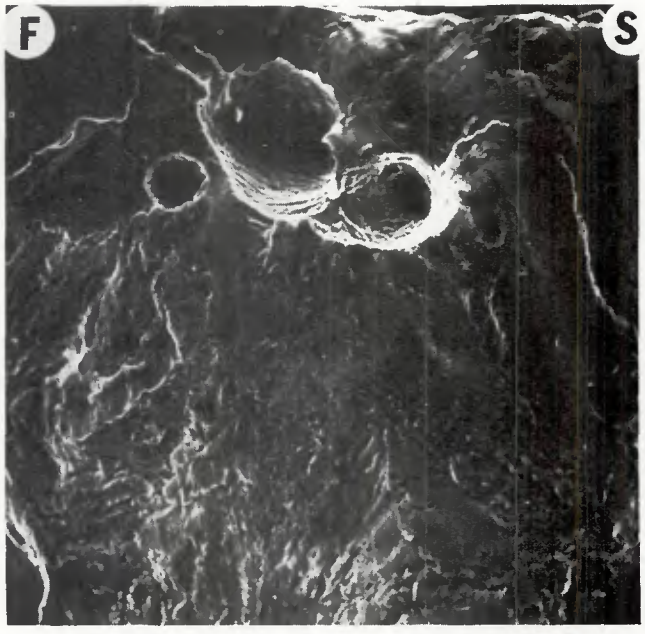

Fig. 8 — Higher magnification view of one of the group of pores responsible for the fatigue fracture surface shown in Fig. 7 (see Fig. 6 for location). FS is one edge of the fracture surface. (X220, reduced 9%)

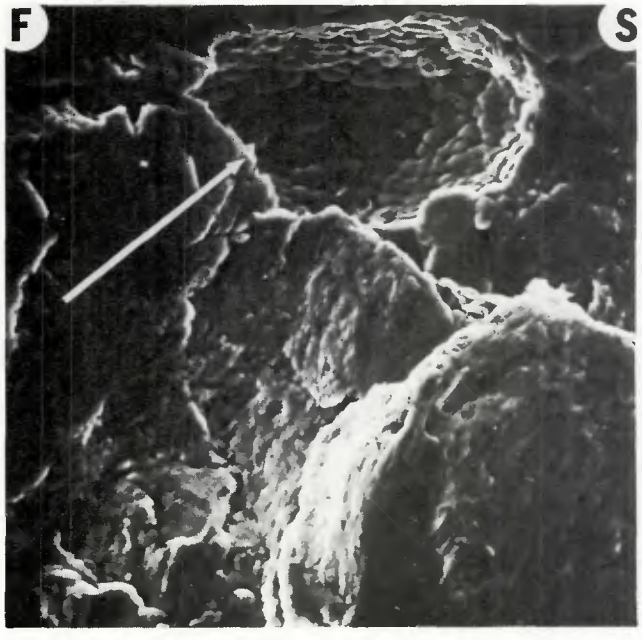

Fig. 9 — Plan view of another of the pores (arrow) responsible for the fatigue fracture surface shown in Fig. 7 (see Fig. 6 for location). FS is one edge of the fracture surface. (X580, reduced 9%)

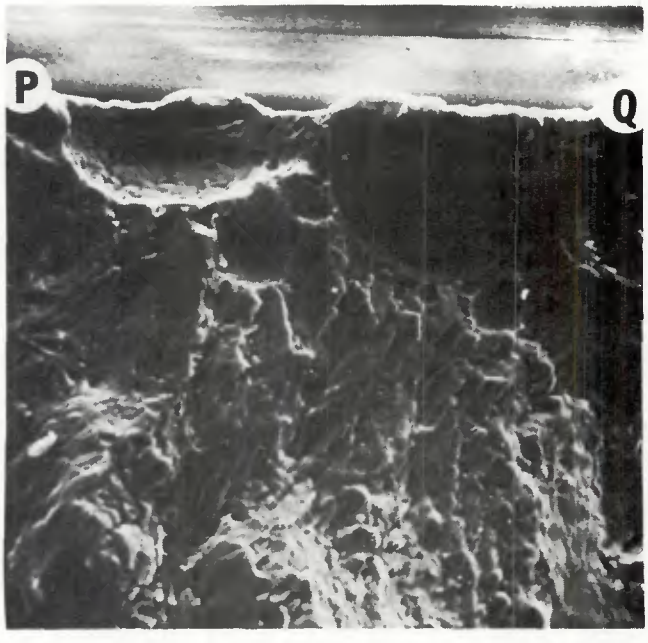

Fig. 10 — Plan view of a second group of pores responsible for the fatigue fracture surface shown in Fig. 7. (see Fig. 6 for location). PQ is one edge of the fracture surface. (X370, reduced 9%)

tional area determined for each fracture surface (Table 1) was plotted against the related fatigue life and a smooth curve obtained (Fig. 13) — the larger the cross sectional area of the initiating site the shorter the life.

Discussion

That the pores responsible for nucleating fatigue cracks in the flexural bending testpieces were all located within one pore diameter of a testpiece surface, and that it was possible to directly relate fatigue life at constant amplitude to the cross sectional area of the crack initiating pores (Fig. 13), indicate that pore location and size as well as total weld porosity content are the primary factors controlling fatigue behavior. Total weld porosity content apparently influences flexural bending fatigue behavior by affecting the probability of one or more pores being situated at or near a testpiece surface, this probability being higher the faster the welding speed. Since welding speed and weld solidification rate are macroscopically equivalent, the number, size and distribution of pores in a weld are apparently controlled, in part, by the solidification rate.

A comparison between the effects of porosity on fatigue behavior reported in this paper and those reported by Rupert and Rudy (Refs. 3,4) and Shore (Ref. 5) is not possible because of differences in the fatigue

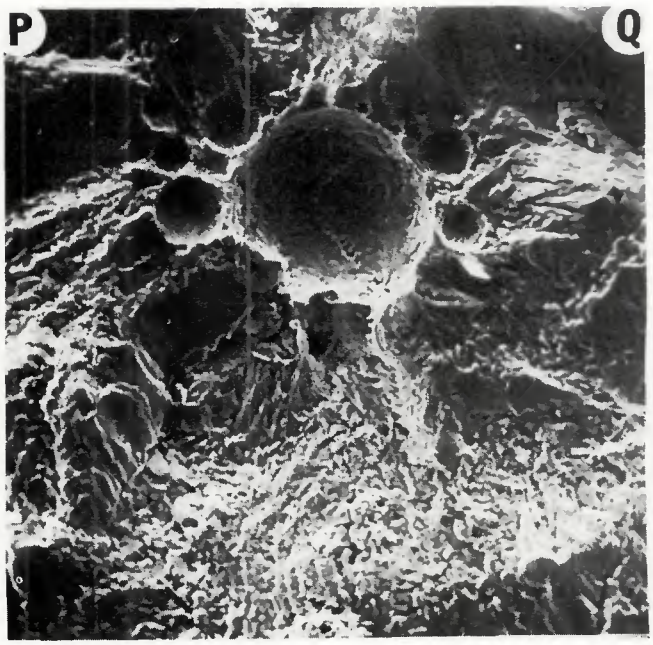

Fig. 11 — Plan view of a third group of pores responsible for the fatigue fracture surface shown in Fig. 7 (see Fig. 6 for location). PQ is one edge of the fracture surface. (X230, reduced 9%)

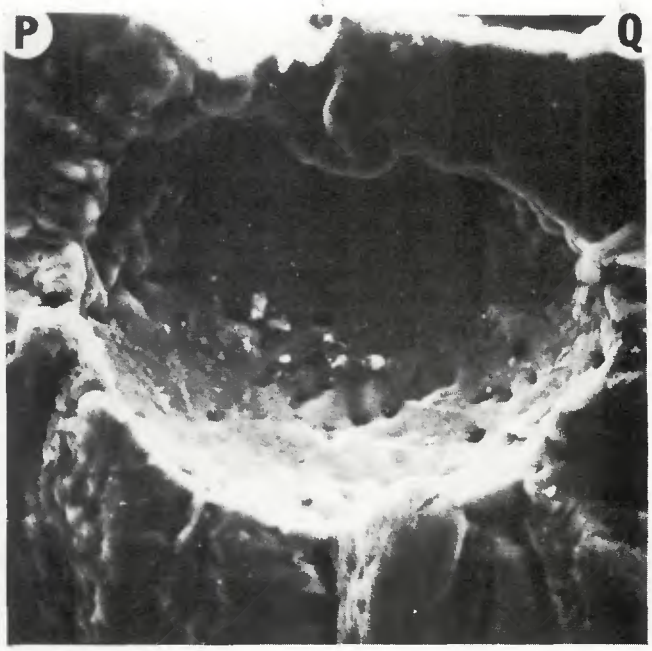

Fig. 12 — Plan view of another pore responsible for the fatigue fracture surface shown in Fig. 7 (see Fig. 6 for location). PQ is one edge of the fracture surface. (X1100, reduced 9%)

testing procedures (flexural bending as opposed to axial tension) and disparity in the weld porosity values; e.g., whereas Rupert and Rudy, and Shore expressed weld porosity as a percentage of the fracture surface area (with percentage porosity values ranging from 0 to 32%), the absolute cross sectional area values determined for the flexural bending fatigue crack initiating sites were very small — ranging from 6.0×10^{-4} to 11.2×10^{-2} mm². The flexural bending fatigue results clearly reveal that, in high quality welds, pores and groups of pores less than 1/64 in. diam can be responsible for substantial reductions in fatigue life (see Table 1). It is interesting to note that single pores and groups of pores greater than 1/64 in. diam were not the cause of any of the flexural bending failures examined under the scanning electron microscope; i.e., pores and groups of pores larger than 1/64 in. diam were nonexistent near the surfaces of the fatigue testpieces.

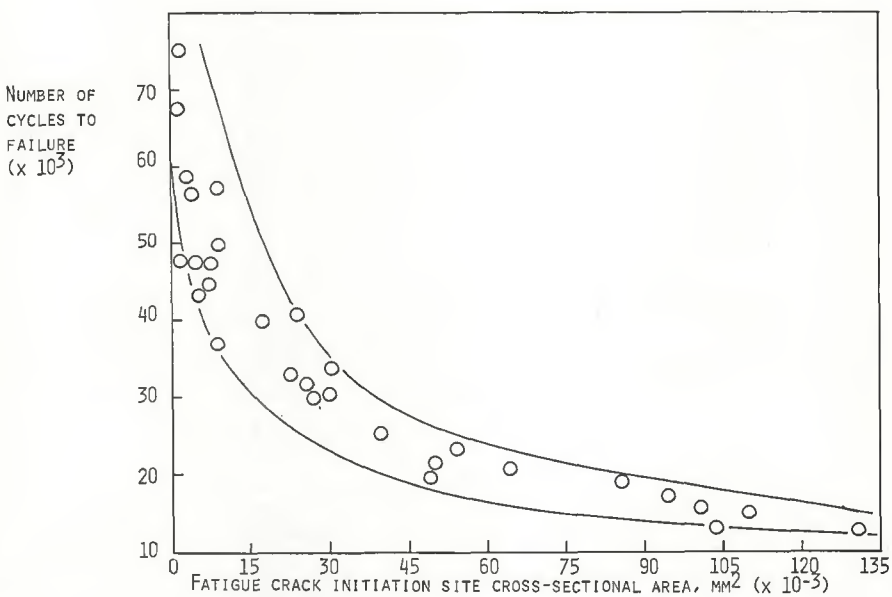

Fig. 13 — Number of cycles to failure of the flexural bending testpieces versus the related fatigue crack initiation site cross sectional area.

Conclusions

1. Flexural bending fatigue life at constant amplitude was directly related to the cross sectional area of the crack initiating pores, the average crack initiating site area increasing with increasing welding speed.

2. Pores as small as 0.1 mm (0.004 in.) caused substantial reductions in the fatigue lives of the flexural bending testpieces.

3. All the pores responsible for the flexural bending crack nucleations were situated within one pore diameter of a testpiece surface. This shows the necessity to take into account pore location as well as pore size when assessing weld fatigue behavior in relation to porosity.

References

1. Stobert, W. E., "Inert Gas Weldment Effects Study," Final Report (January 1966 - June 1966) on Contract NAS8-20168 from Aerospace Group, Quality Control Research Section, The Boeing Company.

2. Martelee, J., *Welding in the World,* 2 (7), 1969, p. 122.

3. Rupert, E. J. and Rudy, J. F., "Analytical and Statistical Study on the Effects of Porosity Level on the Weld Joint Performance," Technical Summary Report on Contract NAS8-11335 from Martin Marietta Corporation, Martin Company, March 1966.

4. Rupert, E. J. and Rudy, J. F., *Welding Journal,* 49 (7), July 1970, Research Suppl., p. 322-s.

5. Shore, R. J., "Effects of Porosity on High Strength Aluminum 7039 Welds," M.Sc. Thesis, Ohio State Univ., 1968.

6. Saperstein, Z. P., Prescott, G. R., and

Monroe, F. H., *Welding Journal*, 43 (10), Oct. 1964, Research Suppl., p. 443-s.

7. Terent'ev, I. M., Barutkin, F. E. and Konoualov, G. S., *Weld Prod.*, 12 (10), 1965, p. 29.

8. Nikiforov, G. D. and Makhortova, E G., Ibid., 8 (4), 1961, p. 12.

9. Kizer, D. E., Saperstein, Z. P. and Schwartzbart, H., "Preparation and Instrumentation for Welding S-1C Components," Phase 1 Report on contract NAS8-20363 from Illinois Institute of Technology, Research Institute, November 1966.

10. Andrew, R. C. "The Effects of Porosity on the Transverse Fatigue Properties of MIG Welds in 5083 Aluminium Alloy," Ph.D. Thesis, University of Queensland, 1972.

11. Waring, J. and Andrew, R. C., *Australian Welding Journal*, 16 (6), 1972, p. 45.

Acknowledgment

Grateful acknowledgment is made to Comalco Limited for their financial support and for their provision of a Post-Graduate Studentship.

WRC Bulletin No. 107 Aug. 1965

(Reprinted April 1972)

Local Stresses in Spherical and Cylindrical Shells Due to External Loadings

by K. R. Wichman, A. G. Hopper and J. L. Mershon

Several years ago, the Pressure Vessel Research Committee sponsored an analytical and experimental research program aimed at providing methods of determining the stresses in pressure vessel nozzle connections subjected to various forms of external loading. The analytical portion of this work was accomplished by Prof. P. P. Bijlaard of Cornell University. Development of the theoretical solutions involved a number of simplifying assumptions, including the use of shallow shell theory for spherical vessels and flexible loading surfaces for cylindrical vessels. These circumstances limited the potential usefulness of the results to d_i/D_i ratios of perhaps 0.33 in the case of spherical shells and 0.25 in the case of cylindrical shells. Since no data were available for the larger diameter ratios, Prof. Bijlaard later supplied data, at the urging of the design engineers, for the values of B = 0.375 and 0.50 (d_i/D_i ratios approaching 0.60) for cylindrical shells. In so doing, Prof. Bijlaard included a specific warning concerning the possible limitations of these data.

Following completion of the theoretical work, experimental work was undertaken in an effort to verify the theory. Whereas this work seemingly provided reasonable verification of the theory, it was limited to relatively small d_i/D_i ratios—0.10 in the case of spherical shells and 0.126 in the case of cylindrical shells. Since virtually no data, either analytical or experimental, were available covering the larger diameter ratios, the Bureau of Ships sponsored a limited investigation of this problem in spheres, aimed at a particular design problem, and the Pressure Vessel Research Committee undertook a somewhat similar investigation in cylinders. Results of this work emphasized the limitations in Bijlaard's data on cylindrical shells, particularly as it applies to thin shells over the "extended range."

Incident to the use of Bijlaard's data for design purposes, it had become apparent that design engineers sometimes have difficulty in interpreting or properly applying this work. As a result of such experience, PVRC felt it desirable that all of Bijlaard's work be summarized in convenient, "cookbook" form to facilitate its use by design engineers. However, before this document could be issued, the above mentioned limitations became apparent presenting an unfortunate dilemma, viz., the data indicate that the data are partially inadequate, but the exact nature and magnitude of the error is not known, nor is any better analytical treatment of the problem available (for cylinders).

Under these circumstances, it was decided that the best course was to proceed with issuing the "cookbook," extending Bijlaard's curves as best as possible on the basis of available test data. This decision was based on the premise that all of the proposed changes would be toward the conservative (or "safe") side and that design engineers would continue to use Bijlaard's extended range data unless some alternative were offered. This paper was therefore presented in the hope that it would facilitate the use of Bijlaard's work by design engineers.

Since the paper was originally issued, a number of minor errors have been discovered and incorporated in revised printings as supplies were exhausted. The third revised printing was issued in April 1972.

The price of Bulletin No. 107 is $3.00. Copies may be ordered from the Welding Research Council, 345 East 47th St., New York, N. Y. 10017.